



RESEARCH ARTICLE

10.1029/2018JC013901

Drivers of Interannual Variability of Summer Mixed Layer Depth in the Southern Ocean Between 2002 and 2011

Key Points:

- Summer MLD changes show a zonally asymmetric response to recent atmospheric forcing
- Summer MLD increased in the Antarctic Zone (AZ) of the Atlantic and Indian Ocean sectors between 2002 and 2011
- Wind forcing dominates over temperature-induced changes in summer MLD

Supporting Information:

- Supporting Information S1

Correspondence to:

E. Panassa,
essowe.panassa@awi.de

Citation:

Panassa, E., Völker, C., Wolf-Gladrow, D., & Hauck, J. (2018). Drivers of interannual variability of summer mixed layer depth in the Southern Ocean between 2002 and 2011. *Journal of Geophysical Research: Oceans*, 123, 5077–5090. <https://doi.org/10.1029/2018JC013901>

Received 14 FEB 2018

Accepted 15 JUN 2018

Accepted article online 26 JUN 2018

Published online 3 AUG 2018

©2018. The Authors.

This is an open access article under the terms of the Creative Commons Attribution-NonCommercial-NoDerivs License, which permits use and distribution in any medium, provided the original work is properly cited, the use is non-commercial and no modifications or adaptations are made.

E. Panassa¹ , C. Völker¹, D. Wolf-Gladrow¹ , and J. Hauck¹ ¹ Alfred-Wegener-Institut Helmholtz Zentrum für Polar- und Meeresforschung (AWI), Bremerhaven, Germany

Abstract Climate change projections indicate that there will be warming and an intensification of westerly winds in the Southern Ocean (SO) in the future. These two forcings potentially have opposing effects on the depth of the surface mixed layer. Here we investigate how interannual to decadal variability of atmospheric surface air temperature (SAT) and zonal wind speed (uwind) impact mixed layer depth (MLD) in the SO (south of 30°S) during summer, the season of main biological activity. We use gridded MLD data from observations and atmospheric reanalysis data of uwind and SAT in the SO to assess summer MLD variability and its potential drivers. With a model-based sensitivity experiment, we quantify the relative contributions of uwind versus SAT forcing on the summer MLD in the decade 2002–2011. Wind-induced changes dominate over temperature-induced changes of the MLD between 2002 and 2011. We find a positive trend of summer MLD in the Antarctic Zone of the Atlantic and Indian Ocean sectors. Our model-based sensitivity study suggests that the summer MLD shows a zonally asymmetric response to recent atmospheric forcing. In the Pacific and Australian sectors, cooling and intensification of uwind jointly result in a deepening of the mixed layer. In the Atlantic and Indian sectors, the MLD responds differently north and south of the Antarctic Polar Front (APF). A deepening south of the APF is caused by the increase in uwind, whereas the decrease in uwind and warming act in concert to result in a shoaling of the MLD north of the APF.

1. Introduction

The Southern Ocean (SO) is a key region for the global carbon cycle and the climate system (Frölicher et al., 2015; Marshall & Speer, 2012). It takes up about 40% of the total anthropogenic carbon that enters the ocean (Gruber et al., 2009; Khatiwala et al., 2009) and is responsible for about 80% of upwelling of nutrient-rich deep waters (Lumpkin & Speer, 2007; Talley, 2013). The cycling of carbon in this region depends on mixed layer (ML) dynamics, wind-driven Ekman transport, and eddy fluxes (Sabine et al., 2004; Sallée et al., 2012; Verdy et al., 2007). ML variability controls the availability of light and nutrients for phytoplankton in spring and summer as well as the grazing pressure by zooplankton (Carranza & Gille, 2015; Fauchereau et al., 2011; Llort et al., 2015; Venables & Moore, 2010). Phytoplankton productivity, in turn, is a main driver of the SO CO₂ uptake in spring and summer (Lenton et al., 2013).

Over the recent decades, observational evidence has revealed a strengthening of the westerly winds in the SO, which is supported by model studies (Marshall, 2003; Swart & Fyfe, 2012; Thompson et al., 2011). This is related to the positive trend in the Southern Annular Mode (SAM) index in response to the complex interaction between the stratospheric ozone depletion and the increase in the atmospheric greenhouse gas concentrations (Abram et al., 2014; Lee & Feldstein, 2013; Thompson et al., 2011). The positive trend in the SAM is expected to induce stronger summer wind stress (Fogt et al., 2009; Thompson et al., 2011), suggesting that the effect of summer wind forcing might dominate over buoyancy forcing with respect to summer mixed layer depth (MLD) variability. With the exception of the SAM trend, recent changes in the high-latitude Southern Hemisphere surface climate can largely be explained by internal climate variability (Jones et al., 2016).

The SO MLD is highly sensitive to climate change and variability (Hauck et al., 2015; Sallée et al., 2010, 2013). It is, however, not clear how the effects of the global warming signal (increased stratification, Gille, 2008) and the wind signal (decreased stratification, Thompson et al., 2011), which occur simultaneously in the SO, will impact ML dynamics in the future (Hauck et al., 2015). It is therefore critical to understand recent effects of wind intensification and temperature trend and variability on ML dynamics.

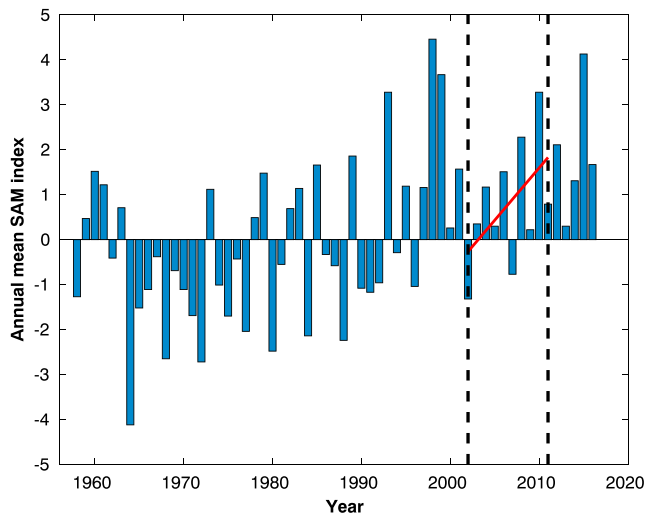


Figure 1. Annual mean time series of the Southern Annular Mode (SAM) index from 1958 to 2016 (Marshall, 2003). The period 2002–2011 on which we focus in this study is emphasized by the two dashed black vertical lines. The red slope line represents the SAM trend that is calculated from the 10 annual SAM index values over the period 2002–2011.

The positive trend in the SAM has led to zonally asymmetric anomalies in MLD caused by heat flux anomalies associated with SAM (Sallée et al., 2010). On longer time scales, we might expect the increase in surface atmospheric temperature to have a stronger effect on the summer MLD than the SAM signal. While SO warming is projected to significantly shoal the summer MLD in the subtropical zone in simulations of the 21st century, a suite of eight models disagrees about the sign of MLD change south of 44°S (Hauck et al., 2015).

During summer, the MLD in the SO is relatively shallow (MLD < 90 m) compared to other seasons because high irradiance and comparatively low wind stress lead to stratification. Strong wind events (summer storms), however, can destabilize the water column profoundly and deepen the ML, which consequently leads to enhanced nutrient (Fe, Si, or nitrate depending on the region) supply from subsurface waters to the euphotic zone and increased phytoplankton productivity (Carranza & Gille, 2015). Mechanisms that drive the summer ML variability in the SO were explored at the subseasonal time scale (Carranza & Gille, 2015).

ML deepening is caused mainly by wind-induced mixing, surface cooling, and/or Ekman pumping driven by the wind stress curl (Carranza & Gille, 2015). The physical mechanisms that link the changes in wind speed with

those in MLD are the turbulent kinetic energy input through the generation and breaking of waves (Denman, 1973). In contrast, temperature impacts MLD by changing the density gradient. The effect of Ekman pumping can change the stratification through the input of denser water.

In this study, we analyze the summer MLD variability in the period 2002–2011 and attempt to unravel whether this variability is dominantly driven by wind or buoyancy forcing. Here we do not distinguish whether the changes are driven by changes in wind speed directly or by changes in wind stress curl (Ekman pumping). Buoyancy forcing refers to variation in temperature. The period 2002–2011 is characterized by a positive phase of the SAM index (Jones et al., 2016), which corresponds to a positive trend in zonal wind speed.

We chose to focus on the summer season because (1) the SAM trend is strongest in summer (Fogt et al., 2009; Thompson et al., 2011), and (2) the CO₂ uptake in the SO is a balance between outgassing in winter and uptake in summer when biology draws down CO₂ (Lenton et al., 2013). Biological production might respond to changes in MLD in the future, and it is neither understood whether the wind or the warming signal will be the dominant driver nor how the variability in the summer MLD will affect the light and nutrient availability in the future (Hauck et al., 2015).

We analyze the decade 2002–2011 because of an insufficient amount of Argo data before 2002, which consequently has very low spatial coverage in the SO (Cabanes et al., 2013). This period was also used to assess the reinvigoration of the SO carbon sink (Landschützer et al., 2015) and to investigate the potential connection between summer MLD and chlorophyll variability at subseasonal time scales (Carranza & Gille, 2015). We therefore focus on the period 2002–2011 in the context of strong interannual to decadal variability (DeVries et al., 2017; Jones et al., 2016; Landschützer et al., 2015). While this time series is not long enough to identify a trend caused by climate change (Jones et al., 2016), it serves as a case study on a period characterized by a positive phase of the SAM index and a positive trend in wind speed (Figure 1). The changes are not necessarily related to climate change but are interpreted as a signal of interannual to decadal variability. There is a general positive trend in SAM over time (Figure 1). Since the 1990s SAM has shifted more often to its high-index polarity, and the time series from January 2002 to December 2011 shows a clear positive trend of the SAM index.

In the first part of our study, we analyzed a global data set derived from observations and remote sensing of summer MLD and its potential drivers (zonal wind speed and near surface air temperature, SAT). In the second part of our study we combined observations with a model-derived sensitivity analysis of MLD to quantify the relative contributions of wind and air temperature forcing to the MLD variability.

2. Data and Methods

2.1. Atmospheric Variables

We used the monthly European Centre for Medium-Range Weather Forecasts ERA-Interim reanalysis for the period 2002–2011 of 10-m zonal surface wind speed (Dee et al., 2011) and 2-m SAT. These are all available on <http://www.ecmwf.int/en/research/climate-reanalysis/era-interim> with a spatial resolution of $1^\circ \times 1^\circ$.

We used the climatological CORE2 atmospheric forcing fields (Large & Yeager, 2009) for our model simulation. This data set includes 6-hourly fields of zonal and meridional wind speed, SAT specific humidity, sea level pressure, shortwave and longwave radiation, and monthly precipitation.

The annual mean SAM index shown in this study (Marshall, 2003) was calculated from the station based index of the SAM based on the difference of sea level pressure fields measured between 40°S and 65°S . The monthly SAM index time series used to estimate the annual mean SAM index started in January 1957 and is ongoing (Marshall, 2003). This data set is available at <https://climatedataguide.ucar.edu/climate-data/marshall-southern-annular-mode-sam-index-station-based>.

2.2. Ocean Variables

We used monthly surface gridded sea surface temperature (SST) fields from European Centre for Medium-Range Weather Forecasts ERA-Interim reanalysis available on <http://www.ecmwf.int/en/research/climate-reanalysis/era-interim>. This data set has a spatial resolution of $1^\circ \times 1^\circ$, and we used the period of 2002 to 2011.

We used also monthly observations of Coriolis Ocean database ReAnalysis, version 4.0 (CORA4.0) gridded 3-D fields and raw individual profile data of in situ temperature and salinity from the CORIOLIS database (Szekely et al., 2016) received from the MyOcean Service Desk (<http://www.myocean.eu/>). The CORA4.0 data set is from a variety of instruments, mainly from Argo floats, expendable bathythermographs, conductivity-temperature-depth, and expendable conductivity-temperature-depth probes, moorings, buoys, and sensors mounted on marine mammal. The quality control and the sequence of processing of this data set is fully described in Cabanes et al. (2013). The spatial resolution is 0.5° in longitude and latitude (global coverage), and the profiles were vertically interpolated on 152 standard levels from the ocean surface to 2,000 m, the maximum depth reached by Argo floats (5-m resolution from surface at the depth of 100 m; 10-m resolution from 100 m to 800 m, and 20-m resolution from 800 m to 2,000 m, Cabanes et al., 2013). The CORA4.0 data set covers the period from 1990 to 2012 from which we extracted the period 2002–2011. The pre-2002 period was not analyzed because of the low spatial coverage of the observations.

For the MLD calculation, we computed the potential density from the raw and gridded CORA4.0 temperature and salinity fields. We chose to use CORA4.0 gridded temperature and salinity fields assuming that the objective analysis methodology (Bretherton et al., 1976) used for the gridding of the CORA4.0 data set is robust. The analysis of variability and the 10-year trend would be flawed by using a time series of individual profiles with major gaps. This is the reason why we chose to use the gridded product. The MLD is defined as the depth z at which the potential density difference $\Delta\sigma(z) = \sigma(z) - \sigma(z_0)$ exceeds a specific threshold value, in our case 0.03 kg/m^3 (de Boyer Montégut et al., 2004) with $z_0 = 10 \text{ m}$ being the reference depth. For the model MLD calculation, we applied the same density criterion as in the analysis of the CORA4.0 data. It is also important to note that although during the decade 2002–2011 the number of observations has increased during the summer season, some regions such as the Ross and Weddell Seas have only sparsely been sampled (see section 3.4.1). Although these gaps were filled in the gridded product using a robust statistical approach, the interpretation of the MLD variability in these zones might still contain high uncertainty.

2.3. Statistical Analyses

For each monthly time series of the variables, namely MLD, zonal wind speed (*u*wind), and SAT from observations, we estimated the mean seasonal cycle of the period 2002–2011 at each grid point and subtracted this mean seasonal cycle from the data to obtain the anomaly. The mean seasonal cycle of, for example, wind data (10 years of monthly data, 120 values) was estimated by averaging each month over the 2002–2011 time period. We then defined the anomaly by subtracting this mean seasonal cycle from each individual month (e.g., January anomaly = January of given year – mean of all Januaries). The same procedure was followed for SAT and MLD time series. We further only used the summer months

(December, January, and February) for the following analysis. Then at each grid point of the anomaly fields we performed the following analyses:

1. A linear regression model was applied to the anomaly data over time using the nonparametric Sen Slope estimator method (Gilbert, 1987), following the example of Kahru et al. (2009). The Sen Slope estimator method that uses the median slope of all lines through pairs of sample points was preferred over the simple least squares regression because the Sen Slope method is robust (insensitive to outliers).
2. MLD (response variable) was regressed against the potential physical drivers uwind and SAT (predictors) using multiple linear regression (MLR) analysis including the interaction between the uwind and SAT and all quadratic terms (equation (S1) in the supporting information). Taking into account the interaction and quadratic terms in our MLD regression model increased the percentage of variance explained slightly (Figure S1), usually less than 10% and occasionally up to 30% depending on location compared to the model with no interaction and quadratic terms. However, the additional terms also increased the complexity of the regression model. The Akaike Information Criterion (AIC, Akaike, 1973) provides a measure of the optimality of models in the sense of a trade-off between the model complexity (measured by the number of model parameters, including the variance of the additive normal noise) and the goodness of fit (measured by the logarithm of the maximum likelihood for the data). Models with lower AIC are more optimal. However, if the magnitude of the difference in AIC is less than 2 the difference is not significant and one should go for the simpler model. In most of the SO, the AIC of the more complex model (with interactions) is larger than that of the simpler model (no interactions, no quadratic terms; Figure S2) or the magnitude of the difference in AIC is less than 2. We therefore, in the main text, show the regression model with no interaction and quadratic terms:

$$\text{MLD} = \beta_0 + \beta_1 * \text{uwind} + \beta_2 * \text{SAT} + \xi \quad (1)$$

where β_0 represents the model intercept, β_1 and β_2 represent the regression coefficient slopes of MLD onto uwind, SAT, and ξ represents the residual.

2.4. Ocean Model

We used the Massachusetts Institute of Technology general circulation model (MITgcm, Marshall et al., 1997). The model solves the primitive equations under the Boussinesq approximation and is discretized on a latitude-longitude-depth Arakawa C grid. Our computational domain is nearly global but excludes the Arctic Ocean (cutoff at 80°N). The latitudinal resolution varies from 0.38° to 2° with the higher resolution in the SO and around the Equator. The longitudinal resolution is constantly 2°. In the vertical, we use 30 vertical layers with 10-m thickness at the surface and the thickness increases gradually with depth to a 500-m thickness to a maximum depth of 5,700 m. The model uses the Gent-McWilliams eddy parameterization (Gent & McWilliams, 1990), sea ice dynamics and thermodynamics (Losch et al., 2010), and the nonlocal K-profile parameterization (KPP) boundary layer mixing scheme (Large et al., 1994) for the vertical mixing within the ML. The physical model setup is the same as is Hauck et al. (2013, 2016). In section 3.4.1 we evaluate the modeled MLD variability.

2.4.1. Sensitivity Experiments

In the following, we describe our approach to evaluate the relative impacts of zonal wind speed and buoyancy forcing on summer MLD with a set of sensitivity experiments using the MITgcm. We followed a two-step approach, in which we first used the model to estimate the sensitivities of MLD to both wind and buoyancy forcing separately. In a second step we multiplied this sensitivity with the observed trends of atmospheric variables to gain insights into the potential change in MLD. The advantage of this approach is that, albeit based on a linearization, it is causal, rather than just based on empirical correlation only, as our data analysis (section 2.3). It is thus better able to separate how much each driver contributes to the MLD trend in the decade 2002–2011.

To estimate the sensitivity of MLD to changes in the zonal wind speed (uwind) or SAT, we first performed a control run with no perturbation applied to simulate oceanic temperature and salinity fields. The model was started from a 100-year spin-up as in Hauck et al. (2016) and run for 4 years. We ran the model by prescribing climatological atmospheric forcing fields from CORE2 (i.e., air temperature, zonal and meridional components of wind speed, sea level pressure, specific humidity, solar radiation, and precipitation). We used bulk formulae (Large & Yeager, 2004) to calculate heat and freshwater fluxes from these forcing fields and from the modeled ocean state.

We perturbed the atmospheric side, namely either SAT or zonal wind speed in sensitivity experiments to change atmospheric heat and fresh water fluxes and to investigate their separate impact on the MLD. The sensitivity runs are identical to the control run, except that we increased either u_{wind} by 0.9 m/s (10% of SO maximum zonal wind) or SAT by 0.2 K (10% of SO maximum summer SAT variability) at every grid point south of 30°S. The perturbation fields were applied separately during the summer season (December, January, and February) only, and we repeated this perturbation for the summer months of the following 2 years. This yields three different perturbed MLD fields from three different years for each variable perturbed.

To obtain the MLD sensitivity fields ($\alpha = \frac{\partial MLD}{\partial u_{wind}}$, $\theta = \frac{\partial MLD}{\partial SAT}$) that represent the effect of each driver on the MLD change, respectively, we calculated the difference between the average of the perturbed MLD fields and the average of the control MLD fields and divided these model MLD anomaly fields by the applied perturbation for each year ($\frac{\partial MLD}{\partial driver} = \frac{MLD_{perturbed} - MLD_{control}}{perturbation}$). In the following, we used the average of the model-derived MLD sensitivity fields from the three summer seasons.

Finally, we combined the model-derived MLD sensitivity fields to atmospheric forcing changes with the observed trends of these drivers. To do so, we linearized the summer MLD trend over the period 2002–2011 by multiplying the averaged MLD sensitivity field with the observed trend of the respective driver:

$$\Delta MLD = \frac{\partial MLD}{\partial u_{wind}} \Delta u_{wind} + \frac{\partial MLD}{\partial SAT} \Delta SAT + \xi \quad (2)$$

Here Δu_{wind} and ΔSAT represent the trends of observed u_{wind} and SAT over the period 2002–2011, respectively, which were all derived from ERA-Interim reanalysis data (zonal wind speed and SAT), while the partial derivatives are the model-derived fields of MLD sensitivities (coefficient of linearization). ξ represents the residual term, and ΔMLD is the observed MLD trend.

We chose to perturb zonal wind speed (rather than total wind speed) as the zonal component constitutes the largest part of the wind speed on monthly time scales in the SO and thereby has a major share in the MLD response. The zonal component is predicted to become stronger in the future (Thompson et al., 2011), whereas the meridional component is smaller and not predicted, to the best of our knowledge, to change in the future. We found that regressions of zonal and of total wind speed on MLD have similar patterns and amplitudes (not shown), and we conclude that the results of our sensitivity experiments are insensitive to whether one chooses zonal or total wind speed.

We also performed the sensitivity experiment with a perturbed precipitation field ($2 \cdot 10^{-9}$ m/s, 10% of SO mean precipitation). The contribution of precipitation to the MLD trend reaches at most $2.7 \cdot 10^{-6}$ m/year, which is 6 orders of magnitude lower than the MLD trends we estimated from u_{wind} or SAT. Therefore, we neglect the effect of precipitation in the following.

3. Results

In the following section, we refer to the Antarctic Zone (AZ) as south of the Antarctic Polar Front (APF), to the Subtropical Zone (STZ) as north of the Subtropical Front (STF), and to the Antarctic Circumpolar Current (ACC) as the zone between the APF and STF. The different sectors of the SO are defined as Atlantic (70°W–20°E), Indian (20–120°E), Australia (120–150°E), and Pacific (150°E–70°W); see Figure 2.

3.1. Variability of MLD, Zonal Wind Speed, and Air Temperature

Maps of the standard deviation of summer zonal wind speed (u_{wind}), SAT, and MLD are shown in Figure 2 for the period of 2002–2011. Summer u_{wind} exhibits the highest variability (2 to 3 m/s; approximately 10% of the mean) in the AZ (south of the APF) and in the STZ (north of the STF) of the Indian sector of the SO (Figure 2a). In contrast, the variability of SAT is lowest in the AZ. Although the variability in SAT is strong (>1.5 K, Figure 2b) in the STZ of the Atlantic and Pacific sectors and close to the Antarctic coast, the MLD in these regions shows weak variability (<10 m; Figure 2c). In contrast, relatively strong MLD variability (15 to 30 m) occurs in the ACC region and the AZ. In the following we intend to unravel whether this variability contains a significant linear trend and whether we can relate the variability of summer MLD to the variability in u_{wind} and SAT.

3.2. Linear Trend Analysis

Summer trend maps of zonal wind speed (u_{wind}), SAT, and MLD are shown in Figure 3 for the period of 2002–2011. A strong positive trend in u_{wind} (up to $0.2 \text{ m}\cdot\text{s}^{-1}\cdot\text{year}^{-1}$) occurs in the Pacific sector

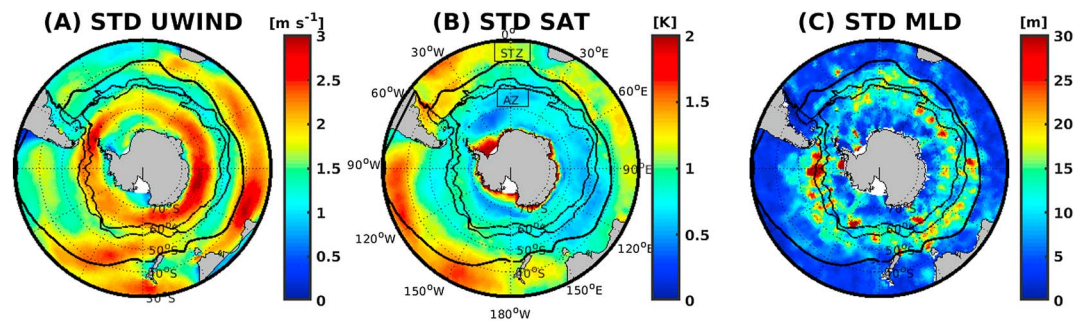


Figure 2. Standard deviation for the period 2002–2011 of the summer (a) zonal wind speed (uwind) from the ERA-Interim reanalysis (Dee et al., 2011), (b) surface air temperature (SAT) from the ERA-Interim reanalysis, and (c) mixed layer depth (MLD) from the CORA4.0 data set (Cabanes et al., 2013). The black contours represent the mean positions of the STF, SAF, and APF (from north to south), respectively (Orsi et al., 1995). In Figure 2b, we labeled Antarctic Zone (AZ, south of the Antarctic Polar Front, APF) and the Subtropical Zone (STZ, north of the Subtropical Front, STF).

of the Subantarctic Zone (SAZ; between the Subantarctic Front, SAF, and STF Figure 3a). The cross-calibrated multiplatform wind product (CCMP; Atlas et al., 2011) winds show similar trends to ERA-Interim (figure not shown). A significant positive trend in SAT occurs in the ACC region of the Atlantic sector and a negative trend is located south of the SAF in the Australian sector. A significant decrease in SAT of up to 0.1 K/year is observed in one patch spanning the Polar Frontal Zone (PFZ, between the APF and SAF), SAZ, and AZ of the Pacific Ocean (Figure 3b). The trend in SST (Figure S3) shows a similar pattern as that in SAT; however, it shows a warming trend close to the Antarctic coast in contrast to SAT.

There is a significant and positive trend of the MLD in the AZ of the Atlantic and Indian sectors. Some patches of significant positive trends occur also in the Pacific and Indian sectors of the PFZ and SAZ (Figure 3c). A significant negative trend occurs in the ACC region of the Indian sector.

The regions of strong ML deepening (regionally up to 2 m/year) co-occur with the regions where we observe a strong increase in uwind and fit partially with the zones where significant cooling occurs in the near-surface atmosphere. In the next section we test whether the variability in uwind and SAT can explain the MLD variability.

3.3. MLR Analysis

In this section, we investigate the impact of summer zonal wind speed (uwind) and SAT variability on the observed summer MLD variability in the period of 2002 to 2011 by regressing the MLD anomalies against the uwind and SAT anomalies.

We find that MLD anomalies are positively correlated with uwind in the ACC region (Figure 4a). This signal extends further north to the STF in the eastern Pacific sector. An increase of the MLD of 2–5 m in the ACC

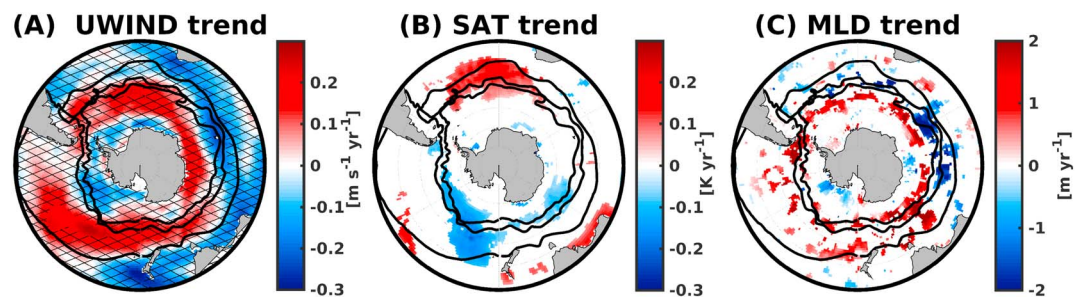


Figure 3. Summer trend for the period 2002–2011 of (a) the zonal wind speed (uwind) from the ERA-Interim reanalysis (Dee et al., 2011), (b) 2-m surface air temperature (SAT) from the ERA-Interim reanalysis, and (c) mixed layer depth (MLD) from the CORA4.0 data set (Cabanes et al., 2013). The wind speed trends that are not significant on the 95% level are overlain with hatching to show the tendency despite the dominance of interannual variability. The black contours represent the mean positions of the STF, SAF, and APF (from north to south), respectively (Orsi et al., 1995). Only significant trends on the 95% confidence level are shown for SAT and MLD. STF = Subtropical Front; SAF = Subantarctic Front; APF = Antarctic Polar Front.

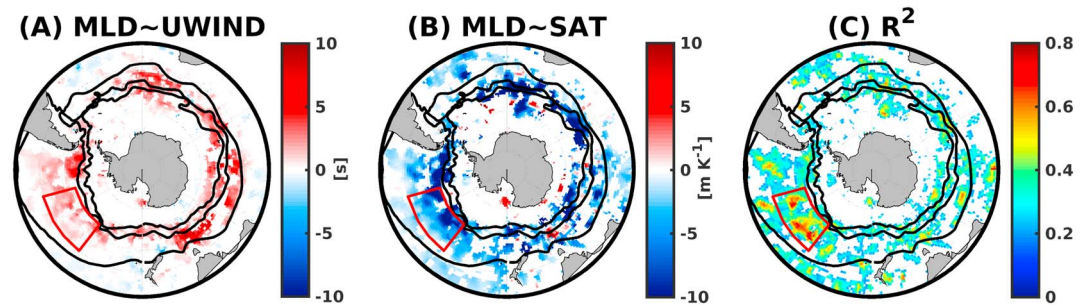


Figure 4. Shown are the regression coefficients of the multilinear regression of observed MLD anomalies during summer months against anomalies during summer months of (a) zonal wind speed (uwind) and (b) surface air temperature (SAT) anomalies. In Figure 4c, we show the explained variance in MLD variability from both uwind and SAT variability (r -square). Only significant regression coefficients on the 95% level are shown. The black contours represent the mean positions of the STF, SAF, and APF (from north to south; Orsi et al., 1995). The red box shown in the figure represents the areas where we integrated uwind, SAT, and MLD anomalies over time, and quantified their temporal relationship as a time series (Figure 5). MLD = mixed layer depth.

region is associated with a 1 m/s increase in uwind. In contrast, MLD anomalies are negatively correlated with SAT (Figure 4b). A decrease of the MLD of 5–10 m is associated with a 1 K increase in SAT. Only few patches show an increase of MLD when SAT increases. The regions, where the regression coefficients of MLD against uwind and against SAT are significant, overlap widely, but the regression coefficients have different signs. The combined effect of uwind and SAT on the MLD can explain up to 80% of its variability (Figure 4c). The highest values of explained variability in MLD ($R^2 > 0.4$) occur in the SAZ of the central and eastern Pacific sector. Generally, more than 40% of the MLD variability is explained by uwind and SAT in the ACC region.

We also examined the relationship between the time series of the spatially averaged MLD, uwind, and SAT anomalies in one region where we found the largest coefficients of determination (R^2) in the central Pacific sector (40–55°S, 142–105°W, the box is shown in Figure 4). In this region, MLD has a negative regression coefficient with respect to SAT, and a 5.5 m deepening of the MLD is associated with a 1 K decrease in SAT (correlation is $R = -0.80$, Figures 5a and 5c). In contrast, MLD has a positive regression coefficient with respect to uwind and an increase of the MLD of 2.5 m is associated with a 1 m/s increase in uwind (correlation is $R = 0.55$, Figures 5b and 5c). Thus, an anomalously deep MLD is associated with anomalously strong uwind and low SAT. The variability in SAT alone can explain about 64% of the variability in the MLD in this region, whereas only 30% of the variability in MLD is explained by uwind alone. When taking into account both effects uwind and SAT, we can explain about 74% of MLD variability. Note that the two effects do not add up.

3.4. Linearization Using Model Sensitivity Experiments

3.4.1. Model Evaluation

How does the model reproduce the summer mean MLD, the MLD seasonal cycle, and trend in comparison to the observations?

The modeled summer mean MLD (Figure 6a) compares reasonably well with the observed values (profiles and gridded data, Figures 6b and 6c). The spatial patterns of summer MLD are reproduced by the model with a reasonable transition between the shallow MLD south of 60°S toward Antarctica, the deep MLD in the ACC region, and the shallow MLD north of the ACC (Figure 6). Nevertheless, the model underestimates the MLD seasonal amplitude in the ACC region.

The climatological seasonal cycles of the MLD averaged south of 30°S from the model and from observations (gridded and individual profiles) are shown in Figure 6d. Similar patterns are observed for the MLD seasonal cycle derived from profile and gridded data (correlation coefficient $R = 0.99$, p value for correlation different from zero <0.05 , $N = 12$). The MLD seasonal cycle from gridded data is approximately 10 m too shallow compared to the one calculated from individual profiles from January to May and 20 m too shallow between June and December. This is in line with the finding of de Boyer Montégut et al. (2004) that the MLD is 25% too shallow when the MLD is calculated using gridded temperature and salinity fields. The model (red dashed line) simulates the observed MLD seasonal cycle (from profiles, black solid line) reasonably well (correlation coefficient $R = 0.98$, p value <0.05 , $N = 12$). However, the model MLD seasonal cycle is too shallow during summer and autumn (on average by 17 m between December and May) and too deep in winter and spring

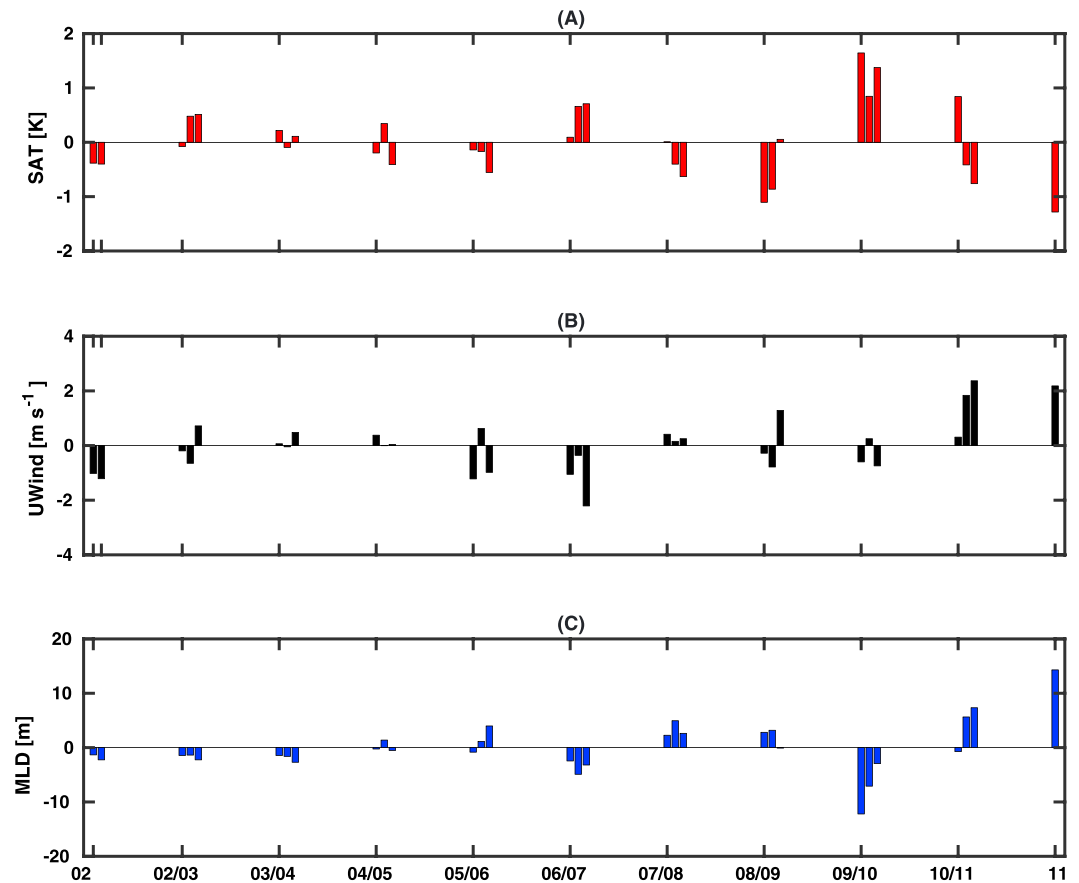


Figure 5. Shown are summer monthly (December to February) area-weighted anomalies of (a) surface air temperature (SAT, red bar), (b) zonal wind speed (uwind, black bar), and (c) the observed MLD (blue bar) in the central Pacific defined in the box (142–105°W, 55–40°S). In the central Pacific the correlation between anomalous MLD and uwind is 0.55, while the correlation between anomalous MLD and SAT is -0.80 . The x axis refers to summer months (DJF) from January 2002 to December 2011. The labels refer to the year. DJF = December–February; MLD = mixed layer depth.

(on average by 25 m between June and November) compared to the observations (profile data). There is no phase shift between the maxima and minima of modeled and observed seasonal cycles. The deepest MLD is found in September and the shallowest in January. The amplitude of the modeled seasonal cycle (155 m) is larger than the amplitudes of the MLD seasonal cycles calculated from observations (profile data: 103 m and gridded data: 91 m). This anomaly is common for general circulation models and is particularly pronounced in the SO. It has been suggested that this discrepancy could be caused by insufficiencies of the vertical mixing parameterization that general circulation models commonly use (Huang et al., 2012; Sen Gupta et al., 2009) or by an excess freshwater flux (Sallée et al., 2013).

As an additional check of the model, we also calculated the summer MLD trend from a hind-cast simulation with the same model setup using the same methodology as for the observational data. We analyzed output from a century-scale simulation where the model is forced by historic atmospheric CO₂ concentrations (Le Quéré et al., 2016) and interannual-varying atmospheric forcing fields from the National Centers for Environmental Prediction/National Center for Atmospheric Research Reanalysis (NCEP/NCAR-R1; Kalnay et al., 1996). The model is spun-up from 1900 to 1947, and we ran the model for 69 years, from 1948 to 2016. This model simulation was submitted to the Global Carbon Budget 2017 and is the same physical set-up as in the Global Carbon Budget 2016 (Le Quéré et al., 2016). The comparison of the modeled MLD trend (Figure 6f) to the observed one (Figure 6e) in the period 2002–2011 shows that the model is able to reproduce the pattern and amplitude of the observed trend in MLD. However, the model shows a smaller number of significant pixels with MLD deepening in the Indian Ocean south of the APF as in the observations.

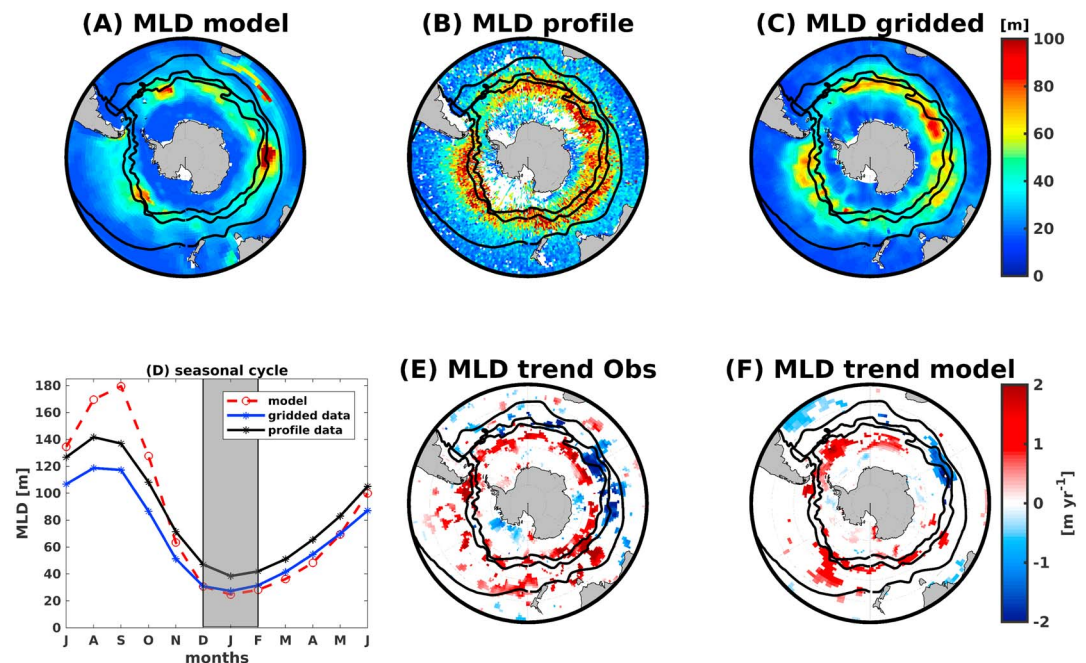


Figure 6. Mean summer (DJF) mixed layer depth (MLD) from (a) model and observations: (b) profile data averaged in $1 \times 1^\circ$ bins and (c) from gridded data, (d) MLD seasonal cycle (average south of 30°S) from model (red dashed line), and observations (from individual temperature and salinity profiles = black solid line; from gridded temperature and salinity data = blue solid line) in the period 2002–2011. In Figure figure6d summer season (DJF) is emphasized in the gray transparent band. Trends in summer of (e) the mixed layer depth from observations (Cabanes et al., 2013) and (f) from the model over the same period 2002–2011. The model was forced by the interannual-varying atmospheric NCEP/NCAR surface wind fields (Kalnay et al., 1996). Only significant trends on the 95% level are shown. The black contours represent the mean positions of the STF, SAF, and APF (from north to south), respectively (Orsi et al., 1995). DJF = December–February; NCAR = National Center for Atmospheric Research; NCEP = National Centers for Environmental Prediction; DJF = December–February; STF = Subtropical Front; SAF = Subantarctic Front; APF = Antarctic Polar Front.

4. Sensitivity Experiments Using the MITgcm

4.1. What Drives the Trend in MLD?

In the following, we attempt to unravel whether wind or buoyancy forcing is responsible for the observed summer MLD trend over the decade 2002–2011. We combine model results and observations to estimate the relative impacts of summer zonal wind speed and surface air temperature changes on the summer MLD as explained in section 2.4.1. This approach allows us to go beyond regression analysis and to derive causal relationships.

4.1.1. MLD Trend Caused by Wind Changes

The MLD sensitivity to uwind perturbation $\alpha = \frac{\partial \text{MLD}}{\partial u_{\text{wind}}}$ is generally positive, and it is highest ($\alpha > 20$ s) in the ACC region. It is close to zero south of 60°S and north of 35°S (Figure 7a). A strong positive trend in uwind occurs in the the PFZ and SAZ of the Pacific sector and in the AZ of the Atlantic and Indian sectors (Figure 7b, note that this figure is the same as Figure 3a but it includes the nonsignificant parts). A negative trend is found to the north and to the south of the positive trend. The product of the MLD sensitivity to uwind perturbation (α) and the actual observed uwind trend gives an estimate of the wind-induced MLD change (Figure 7c). A shoaling of the ML occurs in the PFZ and the STZ of the Indian sector and in the central PFZ of the Pacific sector. This is caused by the combination of a positive sensitivity α (Figure 7a) and a decrease in uwind (Figure 7b). In contrast, a uwind-driven MLD increase occurs in the SAZ of the Pacific sector and stretches toward the AZ of the Atlantic and Indian sectors. In these regions high positive α values co-occur with an increase in uwind (Figure 7c).

4.1.2. Seasonal MLD Trend Caused by Surface Air Temperature Changes

The MLD sensitivity to SAT perturbation $\theta = \frac{\partial \text{MLD}}{\partial \text{SAT}}$ is generally negative, which leads to a zonally asymmetric SAT-driven MLD trend. θ is strongest ($\theta < -10$ m/K) in the ACC region of the Indian sector (Figure 8a). It is close to zero south of 60°S and north of 35°S . The largest decrease in SAT (< -0.1 K/year) occurs from the AZ

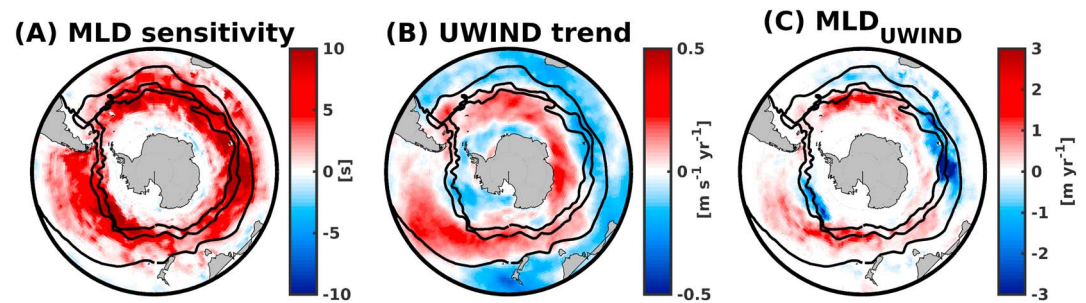


Figure 7. Summer MLD trend estimated from zonal wind (2002–2011). (a) The modeled MLD sensitivity to zonal wind perturbation (α), (b) the zonal wind trends from 2002 to 2011 from the ERA-Interim reanalysis (Dee et al., 2011), and (c) the corresponding summer estimated MLD tendencies obtained by multiplying the corresponding MLD sensitivity to zonal wind perturbation with the respective summer observed zonal wind trends (MLD_{UWIND}). Note that the scale is different for each figure. The black contours represent the mean positions of the STF, SAF, and APF (from north to south), respectively (Orsi et al., 1995). Note that the observed trend (Figure 7b) is not masked to only show the significant parts and that this figure is the same (except for the masking) as Figure 3a. MLD = mixed layer depth; STF = Subtropical Front; SAF = Subantarctic Front; APF = Antarctic Polar Front.

to the SAZ in the eastern and central Pacific sector (Figure 8b, note that this figure is the same as Figure 3b but it includes the nonsignificant parts). This signal extends further eastward to Drake Passage and westward to the Australian sector. Besides a patch in the western Indian sector, the remaining basin shows an increase in SAT. The largest increase in SAT (> 0.1 K/year) occurs in the SAZ of the central Atlantic sector. The product of the MLD sensitivity to SAT perturbation (θ) and the actual observed SAT trend gives an estimate of the SAT-induced MLD change (Figure 8c). Temperature-driven ML deepening occurs in the ACC region of the Pacific and Australian sectors (red in Figure 8c). A temperature-driven ML shoaling occurs in the ACC region of the Atlantic and Indian sectors (blue in Figure 8c).

4.1.3. Combined Effects of Air Temperature and Wind Changes on MLD

The simulated MLD trend from the sensitivity experiment captures the main characteristics of the observed MLD trend (Figures 9a and 9b). The sign of the total MLD trend follows the uwind-induced MLD trend. This signal is modulated by the zonally asymmetric SAT-induced MLD trend that is generally lower in magnitude. The uwind- and SAT-induced MLD trends reinforce each other in the Australian and western Pacific sectors, in the PFZ and SAZ of the Indian sector, and in the SAZ of the Atlantic sector (Figures 7c and 8c). The uwind- and SAT-induced MLD trends oppose each other in the AZ of the Atlantic and Indian sectors and in the AZ and PFZ of the eastern Pacific sector. The uwind-induced MLD trend is, however, stronger than the SAT-induced MLD trend in these regions and dominates the total response. On a SO wide scale, uwind is the dominant factor for the summer MLD trend. Temperature, however, dominates over uwind in the STZ of the Pacific and Indian sectors, and in some Antarctic coastal zones (Figure 10).

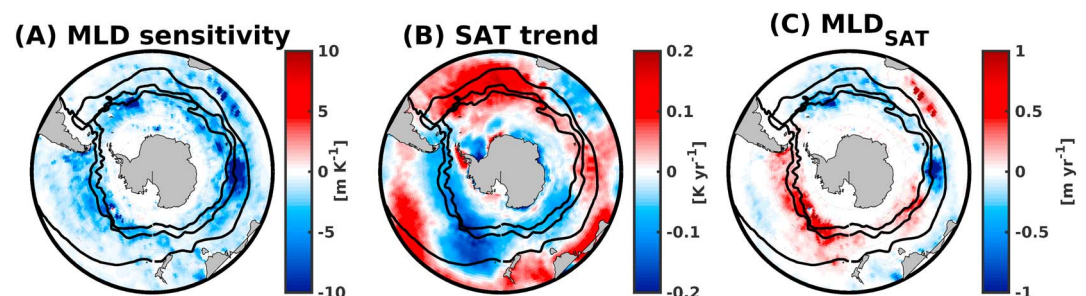


Figure 8. Summer MLD trend estimated from air temperature (2002–2011). (a) The modeled MLD sensitivity to air temperature perturbation (θ), (b) the air temperature trends from 2002 to 2011 from ERA-Interim reanalysis (Dee et al., 2011), and (c) the corresponding summer estimated MLD tendencies obtained by multiplying the corresponding MLD sensitivity to air temperature perturbation with the respective summer observed air temperature trends (MLD_{SAT}). Note that the scale is different for each figure. The black contours represent the mean positions of the STF, SAF, and APF (from north to south), respectively (Orsi et al., 1995). Note that the observed trend (Figure 8b) is not masked to only show the significant parts and that this figure is the same (except for the masking) as Figure 8b. MLD = mixed layer depth; STF = Subtropical Front; SAF = Subantarctic Front; APF = Antarctic Polar Front; SAT = surface air temperature.

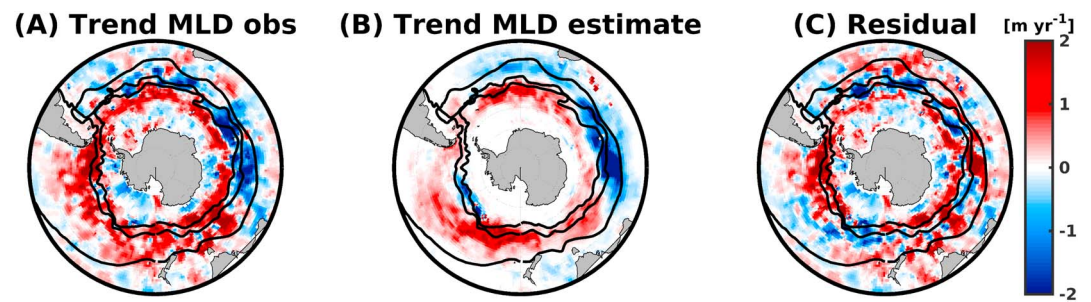


Figure 9. MLD trend from (a) observations, (b) from the product of model sensitivity and trends of zonal wind speed, air temperature, and precipitation, and (c) from the residual for summer over the period of 2002–2011. The black contours represent the mean positions of the STF, SAF, and APF (from north to south), respectively (Orsi et al., 1995). MLD = mixed layer depth; STF = Subtropical Front; SAF = Subantarctic Front; APF = Antarctic Polar Front.

4.1.4. Residual Component

The residuals of the MLR (equation (1); Figure 9c), represent the part of the observed MLD trend that is not explained by summing up the linear MLD trends from uwind and SAT. The linear model (equation (1)) captures the large-scale spatial features of MLD change (Figure 9a); nevertheless, the residuals are on the same order of magnitude as the observed MLD trend (Figure 9c). A large residual suggests that other drivers impact MLD that we do not consider in our model experiment, such as feedbacks to the atmospheric forcing in the ocean and nonlocal advection effects (Carton et al., 2008). Discrepancies might also arise due to the bias existing in the modeled seasonal cycle of the MLD (Figures 6a and 6d). The modeled summer MLD is too shallow in comparison to the observation. Nonlinearities and dependencies between temperature and uwind forcing could also contribute to this residual. The combination of model results with observations gives a much smoother trend than the observations, which might also contribute to the residual.

5. Discussion

The strong variability in the MLD that we detect in and south of the ACC region follows a MLD deepening trend in the period 2002–2011. An exception to this is that the MLD variability observed in the PFZ and SAZ of the Indian sector follows a negative trend. The analysis of MLD variability and trend, and model sensitivity experiments agrees that the change in MLD south of 65°S is insignificant. These findings are in line with a recent estimate of summer MLD variability based on daily observations between 2001 and 2011 (Carranza & Gille, 2015).

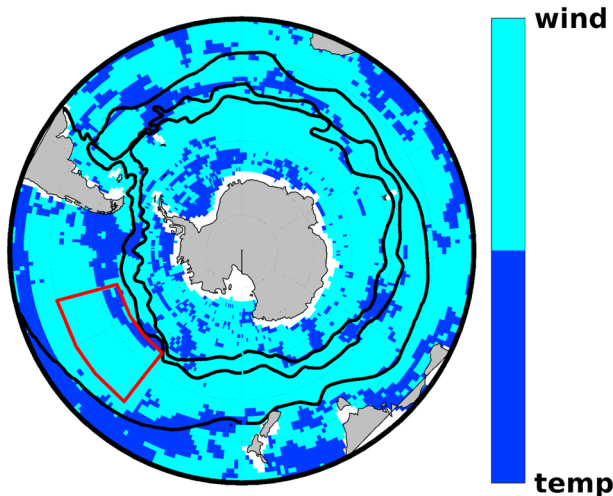


Figure 10. Dominance of driving forces for summer MLD. Cyan color highlights the regions where the wind effect on the MLD change dominates over temperature and the dark blue color shows the regions where the atmospheric temperature forcing on the MLD change dominates over the wind forcing. The black contours represent the mean positions of the STF, SAF, and APF (from north to south), respectively (Orsi et al., 1995). MLD = mixed layer depth; STF = Subtropical Front; SAF = Subantarctic Front; APF = Antarctic Polar Front.

The MLD sensitivity to uwind perturbation in our model is stronger than the sensitivity obtained from the regression analysis (Figures 4a and 6a). In contrast, the MLD sensitivity to SAT is stronger in the regression analysis than in the model (Figures 4b and 7a). This discrepancy could be explained by the fact that the linear regression analysis is based on the assumption of a linear response, whereas the model takes nonlinearities into account. The fact that the model is capable of reproducing the MLD trend by and large suggests that the model captures the sensitivities well. We therefore assign the remaining discrepancy to errors and limitations in the assumptions associated with the multiple regressions analysis (Figure 9a and 9b). This limitation of the statistical analysis might also explain the difference between MLR and model results in the Pacific box (Figure 5). MLR analysis suggests that the temperature effects dominate over uwind in this central Pacific box (Figure 5). The model sensitivity analysis suggests that indeed in the central Pacific, there are areas where temperature effect dominates over uwind effects. However, within the defined Pacific box there are more grid points where uwind effect dominates over temperature effects (Figure 10).

We show only zero-lag responses in our manuscript. Lags of 0 to 12 months were tested in Hauck et al. (2013), and the authors found that the largest response of surface physical variables (current velocity, vertical advection, and SST) occurred immediately (lag zero) and decreased with time. They also showed that analyzing different seasons led to a much larger difference in the response variables than analyzing different lag times. We also tested a lagged regression of summer MLD against zonal wind speed and SST and found the largest response with zero lag (not shown). While longer lag times might be important for the deeper layers (Meredith & Hogg, 2006; Screen et al., 2009), we argue that the immediate atmospheric forcing is more important than the preconditioning of the surface ML in a previous season.

We found a zonal band of ML deepening that is located more to the south in the Indian and Atlantic sectors than in the Pacific. In addition, we found shoaling of the MLD in the Atlantic and Indian sectors north of the areas where MLD increases. This is different from Sallée et al. (2010) who found more a wave-like pattern with a zonal wave number 3. Sallée et al. (2010) however analyzed the annual mean response, whereas we focus on the summer season because of its relevance for biology. We note that we found similar patterns to the one described in Sallée et al. (2010) in autumn and winter (not shown). This suggests that the signal described by Sallée et al. (2010) is dominated by the MLD variability in autumn and winter when the MLD and its variability are larger. Other factors that may contribute to the difference are a slightly different period of analysis and the fact that Sallée et al. (2010) did a regression analysis onto SAM while we analyze the trend over time.

The MLD trend is a combination of a zonally more symmetric response to uwind and a more asymmetric response to SAT. The response of MLD to SAT is in line with warm temperature anomalies in the Atlantic and cold temperature anomalies in the Pacific (Landschützer et al., 2015). The cooling in the Pacific is in line with the long-term cooling trend of SST there (England et al., 2014; Jones et al., 2016). While Landschützer et al. (2015) hypothesize about the stabilization of the surface water in the Pacific and Atlantic sectors, our analyses indicate that there is less stratification south of the APF in the Atlantic and Indian sectors and in large parts of the Pacific sector in summer.

The pattern of the uwind-induced MLD changes in the Atlantic with a positive trend in the AZ and PFZ and negative trend in the SAZ and STZ is in line with the projected poleward shift of the wind speed and MLD maximum (Sen Gupta et al., 2009) in response to a positive trend in SAM index (Abram et al., 2014; Thompson et al., 2011). The shoaling of the MLD in the SAZ and STZ is also supported by the increase in temperature (Figure 7c, Gille, 2008). We acknowledge that our analysis is limited by the number of available observations (Figures S4 and 5). Gap filling is, on the one hand, needed to apply a robust trend analysis, but the resulting trend has a larger uncertainty than calculated from perfect profiles with complete coverage in the SO. We further acknowledge that the trend analysis is sensitive to start and end points (Fay & McKinley, 2013) and that this analysis serves as an example for a period with a positive trend in SAM (Figure 1).

6. Conclusion

Substantial variability in summer MLD is observed in the Antarctic Circumpolar region and the AZ. The decade 2002–2011 is a period where this MLD variability follows a MLD increasing trend in large parts of the AZ south of the APF. There is an asymmetry between MLD changes in the Atlantic and Indian sectors on the one hand and in the Pacific sector on the other hand. In the Pacific and Australian sectors, wind and temperature-induced MLD changes reinforce each other. In contrast, in the AZ of the Atlantic and Indian sectors, the temperature-induced MLD trend counteracts the wind-induced MLD trend, but the wind forcing dominates. The annual mean response of the MLD to positive phases of the SAM (Sallée et al., 2010) differs significantly from the summer response of MLD to perturbations of atmospheric temperature and zonal wind speed. Seasonally resolved analysis is needed to identify how environmental drivers will shape primary production in response to climate change.

References

- Abram, N. J., Mulvaney, R., Vimeux, F., Phipps, S. J., Turner, J., & England, M. H. (2014). Evolution of the Southern Annular Mode during the past millennium. *Nature Climate Change*, 4(7), 564–569. <https://doi.org/10.1038/NCLIMATE2235>
- Akaike, H. (1973). Information theory and an extension of the maximum likelihood principle. In B. N. Petrov & F. Csaki (Eds.), *Second international symposium on information theory* (pp. 267–281). Budapest: Akademiai Kiado.
- Atlas, R., Hoffman, R. N., Ardizzone, J., Leidner, S. M., Jusem, J. C., Smith, D. K., & Gombos, D. (2011). A cross-calibrated, multiplatform ocean surface wind velocity product for meteorological and oceanographic applications. *Bulletin of the American Meteorological Society*, 92(2), 157. <https://doi.org/10.1175/2010BAMS2946.1>

Acknowledgments

We thank the reviewers for their constructive comments that significantly helped to improve this work. We acknowledge open access to the ERA-Interim and CORA4.0 data sets. The ERA-Interim reanalysis data are available on <http://www.ecmwf.int/en/research/climate-reanalysis/era-interim>, and the CORA4.0 data set is made freely available by the Coriolis project and programmes that contribute to it <http://www.coriolis.eu.org>. E. P. and J. H. were funded by the Helmholtz PostDoc Programme PD-102 (Initiative and Networking Fund of the Helmholtz Association).

- Bretherton, F. P., Davis, R. E., & Fandry, C. B. (1976). A technique for objective analysis and design of oceanographic experiments applied to MODE-73. *Deep-Sea Research*, 23(7), 559–582.
- Cabanes, C., Grouazel, A., von Schuckmann, K., Hamon, M., Turpin, V., Coatanoan, C., et al. (2013). The CORA dataset: Validation and diagnostics of in-situ ocean temperature and salinity measurements. *Ocean Science*, 9(1), 1–18. <https://doi.org/10.5194/os-9-1-2013>
- Carranza, M. M., & Gille, S. T. (2015). Southern Ocean wind-driven entrainment enhances satellite chlorophyll-a through the summer. *Journal of Geophysical Research: Oceans*, 120(1), 304–323. <https://doi.org/10.1002/2014JC010203>
- Carton, J. A., Grodsky, S. A., & Liu, H. (2008). Variability of the oceanic mixed layer, 1960–2004. *Journal of Climate*, 21(5), 1029–1047. <https://doi.org/10.1175/2007JCLI1798.1>
- de Boyer Montégut, C., Madec, G., Fischer, A. S., Lazar, A., & Iudicone, D. (2004). Mixed layer depth over the global ocean: An examination of profile data and a profile-based climatology. *Journal of Geophysical Research*, 109, C12003. <https://doi.org/10.1029/2004JC002378>
- DeVries, T., Holzer, M., & Primeau, F. (2017). Recent increase in oceanic carbon uptake driven by weaker upper-ocean overturning. *Nature*, 542(7640), 215–218. <https://doi.org/10.1038/nature21068>
- Dee, D., Uppala, S., Simmons, A., Berrisford, P., Poli, P., Kobayashi, S., et al. (2011). The ERA-Interim reanalysis: Configuration and performance of the data assimilation system. *Quarterly Journal of the Royal Meteorological Society*, 137(656), 553–597. <https://doi.org/10.1002/qj.828>
- Denman, K. (1973). A time-dependent model of the upper ocean. *Journal of Physical Oceanography*, 3(2), 173–184. [https://doi.org/10.1175/1520-0485\(1973\)003<0173:ATDMOT>2.0.CO;2](https://doi.org/10.1175/1520-0485(1973)003<0173:ATDMOT>2.0.CO;2)
- England, M. H., McGregor, S., Spence, P., Meehl, G. A., Timmermann, A., Cai, W., et al. (2014). Recent intensification of wind-driven circulation in the Pacific and the ongoing warming hiatus. *Nature Climate Change*, 4(3), 222–227. <https://doi.org/10.1038/NCLIMATE2106>
- Fauchereau, N., Tagliabue, A., Bopp, L., & Monteiro, P. (2011). The response of phytoplankton biomass to transient mixing events in the Southern Ocean. *Geophysical Research Letters*, 38, L17601. <https://doi.org/10.1029/2011GL048498>
- Fay, A., & McKinley, G. (2013). Global trends in surface ocean pCO₂ from in situ data. *Global Biogeochemical Cycles*, 27, 541–557. <https://doi.org/10.1002/gbc.20051>
- Fogt, R. L., Perlwitz, J., Monaghan, A. J., Bromwich, D. H., Jones, J. M., & Marshall, G. J. (2009). Historical SAM variability. Part II: Twentieth-century variability and trends from reconstructions, observations, and the IPCC AR4 models. *Journal of Climate*, 22(20), 5346–5365. <https://doi.org/10.1175/2009JCLI2786.1>
- Frölicher, T. L., Sarmiento, J. L., Paynter, D. J., Dunne, J. P., Krasting, J. P., & Winton, M. (2015). Dominance of the Southern Ocean in anthropogenic carbon and heat uptake in CMIP5 models. *Journal of Climate*, 28(2), 862–886. <https://doi.org/10.1175/JCLI-D-14-00117.1>
- Gent, P. R., & McWilliams, J. C. (1990). Isopycnal mixing in ocean circulation models. *Journal of Physical Oceanography*, 20(1), 150–155. [https://doi.org/10.1175/1520-0485\(1990\)020<0150:MIOCM>2.0.CO;2](https://doi.org/10.1175/1520-0485(1990)020<0150:MIOCM>2.0.CO;2)
- Gilbert, R. O. (1987). *Statistical methods for environmental pollution monitoring*. John Wiley & Sons.
- Gille, S. T. (2008). Decadal-scale temperature trends in the Southern Hemisphere ocean. *Journal of Climate*, 21(18), 4749–4765. <https://doi.org/10.1175/2008JCLI2131.1>
- Gruber, N., Gloor, M., Mikaloff Fletcher, S. E., Doney, S. C., Dutkiewicz, S., Follows, M. J., et al. (2009). Oceanic sources, sinks, and transport of atmospheric CO₂. *Global Biogeochemical Cycles*, 23, GB1005, 1924–1924. <https://doi.org/10.1029/2008GB003349>
- Hauk, J., Köhler, P., Wolf-Gladrow, D., & Völker, C. (2016). Iron fertilisation and century-scale effects of open ocean dissolution of olivine in a simulated CO₂ removal experiment. *Environmental Research Letters*, 11(2), 024007. <https://doi.org/10.1088/1748-9326/11/2/024007>
- Hauk, J., Völker, C., Wang, T., Hoppema, M., Losch, M., & Wolf-Gladrow, D. A. (2013). Seasonally different carbon flux changes in the Southern Ocean in response to the Southern Annular Mode. *Global Biogeochemical Cycles*, 27, 1236–1245. <https://doi.org/10.1002/2013GB004600>
- Hauk, J., Völker, C., Wolf-Gladrow, D., Laufkötter, C., Vogt, M., Aumont, O., et al. (2015). On the Southern Ocean CO₂ uptake and the role of the biological carbon pump in the 21st century. *Global Biogeochemical Cycles*, 29, 1451–1470. <https://doi.org/10.1002/2015GB005140>
- Huang, C. J., Qiao, F., Shu, Q., & Song, Z. (2012). Evaluating austral summer mixed-layer response to surface wave-induced mixing in the Southern Ocean. *Journal of Geophysical Research*, 117, C00J18. <https://doi.org/10.1029/2012JC007892>
- Jones, J. M., Gille, S. T., Goosse, H., Abram, N. J., Canziani, P. O., Charman, D. J., et al. (2016). Assessing recent trends in high-latitude Southern Hemisphere surface climate. *Nature Climate Change*, 6(10), 917–926. <https://doi.org/10.1038/NCLIMATE3103>
- Kahru, M., Kudela, R., Manzano-Sarabia, M., & Mitchell, B. G. (2009). Trends in primary production in the California Current detected with satellite data. *Journal of Geophysical Research*, 114, C02004. <https://doi.org/10.1029/2008JC004979>
- Kalnay, E., Kanamitsu, M., Kistler, R., Collins, W., Deaven, D., Gandin, L., et al. (1996). The NCEP/NCAR 40-year reanalysis project. *American Meteorological Society*, 77(3), 437–471. [https://doi.org/10.1175/1520-0477\(1996\)077<0437:TNYRP>2.0.CO;2](https://doi.org/10.1175/1520-0477(1996)077<0437:TNYRP>2.0.CO;2)
- Khatiwal, S., Primeau, F., & Hall, T. (2009). Reconstruction of the history of anthropogenic CO₂ concentrations in the ocean. *Nature*, 462(7271), 346–349. <https://doi.org/10.1038/nature08526>
- Landschützer, P., Gruber, N., Haumann, F. A., Rödenbeck, C., Bakker, D. C., Van Heuven, S., et al. (2015). The reinvigoration of the Southern Ocean carbon sink. *Science*, 349(6253), 1221–1224. <https://doi.org/10.1126/science.aab2620>
- Large, W. G., McWilliams, J. C., & Doney, S. C. (1994). Oceanic vertical mixing: A review and a model with a nonlocal boundary layer parameterization. *Reviews of Geophysics*, 32(4), 363–403. <https://doi.org/10.1029/94RG01872>
- Large, W. G., & Yeager, S. G. (2004). Diurnal to decadal global forcing for ocean and sea-ice models: The data sets and flux climatologies. *NCAR Technical Note* (112 pp.). Boulder, CO: National Center for Atmospheric Research.
- Large, W., & Yeager, S. (2009). The global climatology of an interannually varying air–sea flux data set. *Climate Dynamics*, 33(2–3), 341–364. <https://doi.org/10.1007/s00382-008-0441-3>
- Le Quééré, C., Andrew, R. M., Canadell, J. G., Sitch, S., Korsbakken, J. I., Peters, G. P., et al. (2016). Global carbon budget 2016. *Earth System Science Data*, 8(2), 605. <https://doi.org/10.5194/essd-8-605-2016>
- Lee, S., & Feldstein, S. B. (2013). Detecting ozone-and greenhouse gas-driven wind trends with observational data. *Science*, 339(6119), 563–567. <https://doi.org/10.1126/science.1225154>
- Lenton, A., Tilbrook, B., Law, R., Bakker, D. C., Doney, S. C., Gruber, N., et al. (2013). Sea-air CO₂ fluxes in the Southern Ocean for the period 1990–2009. *Biogeosciences Discussions*, 10, 285–333. <https://doi.org/10.5194/bgd-10-285-2013>
- Llort, J., Lévy, M., Sallée, J.-B., & Tagliabue, A. (2015). Onset, intensification, and decline of phytoplankton blooms in the Southern Ocean. *ICES Journal of Marine Science*, 72(6), 1971–1984. <https://doi.org/10.1093/icesjms/fsv053>
- Losch, M., Menemenlis, D., Campin, J.-M., Heimbach, P., & Hill, C. (2010). On the formulation of sea-ice models. Part 1: Effects of different solver implementations and parameterizations. *Ocean Modelling*, 33(1), 129–144. <https://doi.org/10.1016/j.ocemod.2009.12.008>
- Lumpkin, R., & Speer, K. (2007). Global ocean meridional overturning. *Journal of Physical Oceanography*, 37(10), 2550–2562. <https://doi.org/10.1175/JPO3130.1>
- Marshall, G. J. (2003). Trends in the Southern Annular Mode from observations and reanalyses. *Journal of Climate*, 16(24), 4134–4143. [https://doi.org/10.1175/1520-0442\(2003\)016<4134:TITSAM>2.0.CO;2](https://doi.org/10.1175/1520-0442(2003)016<4134:TITSAM>2.0.CO;2)

- Marshall, J., Adcroft, A., Hill, C., Perelman, L., & Heisey, C. (1997). A finite-volume, incompressible Navier-Stokes model for studies of the ocean on parallel computers. *Journal of Geophysical Research*, *102*(C3), 5753–5766. <https://doi.org/10.1029/96JC02775>
- Marshall, J., & Speer, K. (2012). Closure of the meridional overturning circulation through Southern Ocean upwelling. *Nature Geoscience*, *5*(3), 171–180. <https://doi.org/10.1038/NGEO1391>
- Meredith, M. P., & Hogg, A. M. (2006). Circumpolar response of Southern Ocean eddy activity to a change in the Southern Annular Mode. *Geophysical Research Letters*, *33*, L16608. <https://doi.org/10.1029/2006GL026499>
- Orsi, A. H., Whitworth, T., & Nowlin, W. D. (1995). On the meridional extent and fronts of the Antarctic Circumpolar Current. *Deep Sea Research Part I: Oceanographic Research Papers*, *42*(5), 641–673. [https://doi.org/10.1016/0967-0637\(95\)00021-W](https://doi.org/10.1016/0967-0637(95)00021-W)
- Sabine, C. L., Feely, R. A., Gruber, N., Key, R. M., Lee, K., Bullister, J. L., et al. (2004). The oceanic sink for anthropogenic CO₂. *Science*, *305*(5682), 367–371. <https://doi.org/10.1126/science.1097403>
- Sallée, J.-B., Matear, R. J., Rintoul, S. R., & Lenton, A. (2012). Localized subduction of anthropogenic carbon dioxide in the Southern Hemisphere oceans. *Nature Geoscience*, *5*(8), 579–584. <https://doi.org/10.1038/ngeo1523>
- Sallée, J.-B., Shuckburgh, E., Bruneau, N., Meijers, A., Bracegirdle, T., & Wang, Z. (2013). Assessment of Southern Ocean mixed-layer depths in CMIP5 models: Historical bias and forcing response. *Journal of Geophysical Research: Oceans*, *118*, 1845–1862. <https://doi.org/10.1002/jgrc.20157>
- Sallée, J., Speer, K., & Rintoul, S. (2010). Zonally asymmetric response of the Southern Ocean mixed-layer depth to the Southern Annular Mode. *Nature Geoscience*, *3*(4), 273–279. <https://doi.org/10.1038/ngeo812>
- Screen, J. A., Gillett, N. P., Stevens, D. P., Marshall, G. J., & Roscoe, H. K. (2009). The role of eddies in the Southern Ocean temperature response to the Southern Annular Mode. *Journal of Climate*, *22*(3), 806–818. <https://doi.org/10.1175/2008JCLI2416.1>
- Sen Gupta, A., Santoso, A., Taschetto, A. S., Ummenhofer, C. C., Trevena, J., & England, M. H. (2009). Projected changes to the Southern Hemisphere ocean and sea ice in the IPCC AR4 climate models. *Journal of Climate*, *22*(11), 3047–3078. <https://doi.org/10.1175/2008JCLI2827.1>
- Swart, N., & Fyfe, J. (2012). Observed and simulated changes in the Southern Hemisphere surface westerly wind-stress. *Geophysical Research Letters*, *39*, L16711. <https://doi.org/10.1029/2012GL052810>
- Szekely, T., Gouillon, J., Pouliquen, S., & Reverdin, G. (2016). CORA, Coriolis Ocean Dataset for Reanalysis. SEANOE. <https://doi.org/10.17882/46219>
- Talley, L. D. (2013). Closure of the global overturning circulation through the Indian, Pacific, and Southern Oceans: Schematics and transports. *Oceanography*, *26*(1), 80–97. <https://doi.org/10.5670/oceanog.2013.07>
- Thompson, D. W., Solomon, S., Kushner, P. J., England, M. H., Grise, K. M., & Karoly, D. J. (2011). Signatures of the Antarctic ozone hole in Southern Hemisphere surface climate change. *Nature Geoscience*, *4*(11), 741–749. <https://doi.org/10.1038/NGEO1296>
- Venables, H., & Moore, C. M. (2010). Phytoplankton and light limitation in the Southern Ocean: Learning from high-nutrient, high-chlorophyll areas. *Journal of Geophysical Research*, *115*, C02015. <https://doi.org/10.1029/2009JC005361>
- Verdy, A., Dutkiewicz, S., Follows, M., Marshall, J., & Czaja, A. (2007). Carbon dioxide and oxygen fluxes in the Southern Ocean: Mechanisms of interannual variability. *Global Biogeochemical Cycles*, *21*, GB2020. <https://doi.org/10.1029/2006GB002916>